THE JOURNAL OF PHYSICAL CHEMISTRY B LETTERS

2005, *109,* 11083−11087
Published on Web 05/13/2005

Controlled Texturing Modifies the Surface Topography and Plasmonic Properties of Au Nanoshells

Hui Wang,[†,||] Glenn P. Goodrich,[‡,||] Felicia Tam,[§,||] Chris Oubre,[§,||] Peter Nordlander,[‡,§,||] and Naomi J. Halas*[,†,‡,||]

Department of Chemistry, Department of Electrical and Computer Engineering, Department of Physics and Astronomy, and the Laboratory for Nanophotonics, Rice University, Houston, Texas 77005

Received: March 21, 2005; In Final Form: April 28, 2005

We report a facile and controllable method for the postfabrication texturing of the surface topography of Au nanoshells based on site-selective chemical etching of the polycrystalline Au nanoshell surface by a bifunctional alkanethiol molecule, cysteamine. This nanoscale surface texturing process systematically introduces dramatic changes to the plasmonic properties of the Au nanoshells. The modification of the plasmon resonant properties of nanoshells as a function of increased surface roughness was examined experimentally and modeled theoretically using three-dimensional finite difference time domain (FDTD) simulations.

Over the past decade, metals have emerged as highly useful materials for a new class of photonic components that control and manipulate light at the nanometer scale.[1−4] Major efforts have been devoted to the design, fabrication, and patterning of metallic nanostructures with controllable sizes and shapes due to the size- and shape-dependent plasmon-derived optical properties such nanostructures possess. The "bottom-up" chemical synthesis of nanoparticles from molecular precursors has provided one very successful approach to the controlled fabrication of a wide variety of metallic nanostructures, such as rods,[5−7] disks,[8−10] triangular plates,[11,12] cubes,[13] caps or cups,[14,15] and branched nanocrystals.[16,17] An alternative approach to tailoring the structure and geometry and thereby manipulating the plasmonic properties of metallic nanostructures involves controlled modification of the metallic structures following fabrication.[18−22] Here we examine how a controlled chemical method for nanoscale texturing of the surface of silica−Au core−shell nanoparticles systematically introduces dramatic changes to their plasmon-derived optical properties.

Metallic nanoshells are, in essence, versatile subwavelength optical components with the remarkable property that their surface plasmon resonance can be tuned across the visible and near-infrared spectral regions by varying the relative dimensions of their core and shell layers.[23] Precise, quantitative agreement between the core and shell dimensions of nanoshells and their plasmon-derived optically resonant properties has been confirmed at the single nanoparticle level.[24] The tunability of nanoshell plasmons can be further extended into the far-infrared by use of the concentric nanoshell, or "nano-matryushka" geometry.[25,26] The plasmon tunability of nanoshells presents a unique approach to the systematic control of optical frequency fields at the nanometer scale, for applications such as surface enhanced spectroscopies.[27−29] Tuning the nanoshell plasmon to the near-infrared "water window" where tissue and blood are transparent has enabled several new biomedical applications, such as whole-blood immunoassays,[30] optically triggerable drug delivery,[31] high-resolution bioimaging,[32] and photothermal cancer therapy.[33]

Here we describe a method for controllably texturing the surface topography and tailoring the plasmonic properties of Au nanoshells based on site-selective chemical etching of the polycrystalline Au nanoshell surface by a bifunctional alkanethiol molecule, cysteamine. Nanostructures treated in this manner present a unique opportunity to carefully examine how nanoscale changes in the surface morphology of a metallic nanostructure may affect both its near- and far-field optical properties. Because the surface plasmon resonance of Au nanoshells is sensitively dependent upon the relative dimensions of the core and shell, the etching process can be monitored by visible−near-infrared (vis−NIR) spectroscopic measurements. Changes in the structure of the nanoshells during the etching process are easily detected by monitoring changes in the plasmon peak wavelength and line shape. Figure 1A shows the time-dependent vis−NIR spectra of a Au nanoshell film immersed in a 50 mM cysteamine solution. The plasmon peak progressively red shifts and decreases in intensity as the immersion time increases until the nanoshell plasmon peak is no longer observable after 120 min. The long wavelength shoulders present in all these spectra are due to the presence of a small quantity of nanoshell aggregates on the film.[34] Because the core dimensions do not change in this process, the red shift of the plasmon peak can be explained by a decrease in the Au shell thickness.[23] The time dependent spectroscopic measurements were also correlated with scanning electron microscopy (SEM) observations, which confirm that the average outer diameter of the nanoshells decreases as the etching time

* To whom correspondence should be addressed. E-mail: halas@rice.edu. Tel: 1-(713) 348-5611. Fax: 1-(713) 348-5686.
[†] Department of Chemistry.
[‡] Department of Electrical and Computer Engineering.
[§] Department of Physics and Astronomy.
[||] Laboratory for Nanophotonics.

10.1021/jp051466c CCC: $30.25

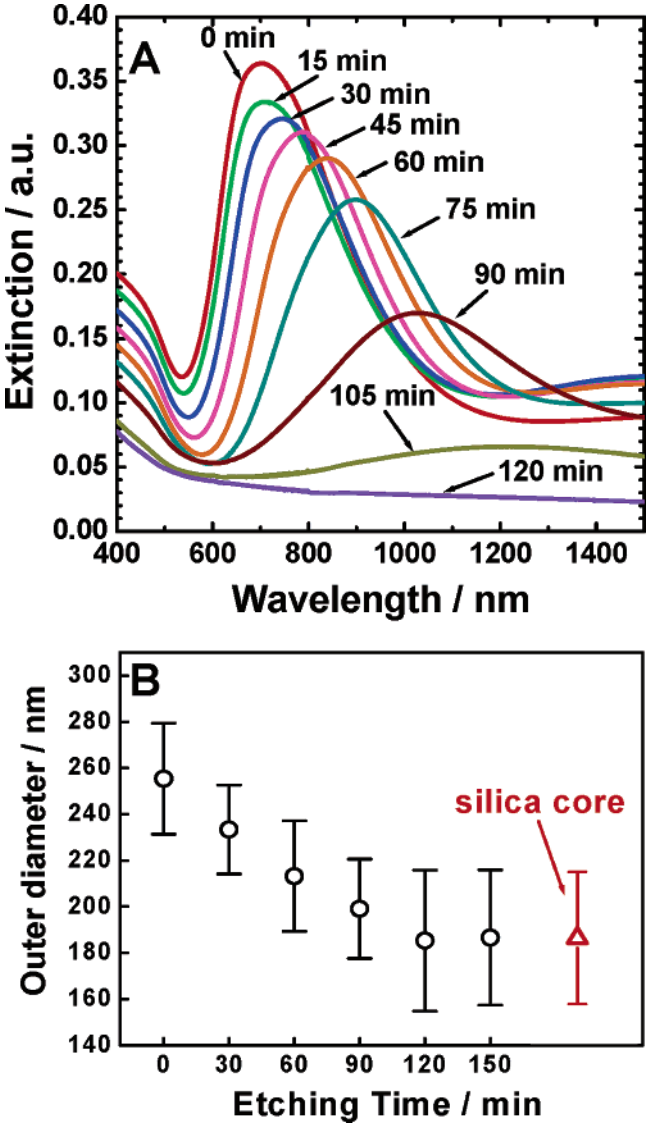

Figure 1. Monitoring of the etching of Au nanoshells by extinction spectroscopy and SEM measurements: (A) Time-dependent vis−NIR spectra of a gold nanoshell (average core radius of 93 nm and shell thickness of 35 nm) film immersed in 50 mM cysteamine solution. The nanoparticle density was nominally 1.5×10^6 nanoshells/mm^2 on the glass substrates. (B) Change in the outer diameters of the gold nanoshells immersed in 50 mM cysteamine solution, obtained directly from the SEM images. The data spots denote the average diameters of the nanoparticles and the error bars correspond to the standard deviations in this measurement.

increases, approaching the diameter of the bare silica cores after 120 min (Figure 1B).

High-resolution SEM provides detailed images of the morphological changes of the nanoshell surface during the etching process. Other structural characterization methods, such as atomic force microscopy, were not able to yield images of the local nanoscale morphology as detailed as this imaging method. After a 1 h exposure in cysteamine, the surface of freshly prepared nanoshells (Figure 2A,B) shows a significant increase in roughness and a large number of hills and valleys randomly arranged over the nanoshell surface can clearly be seen (Figure 2C,D). After 120 min, large pits and fissures have broken up the shell layer, and isolated Au islands are visible on the surface of the silica core (Figure 2E,F). At this stage, because the continuous core−shell structure is no longer maintained, the plasmon peak corresponding to the Au nanoshells is greatly modified. However, there is still a broad and weak absorption

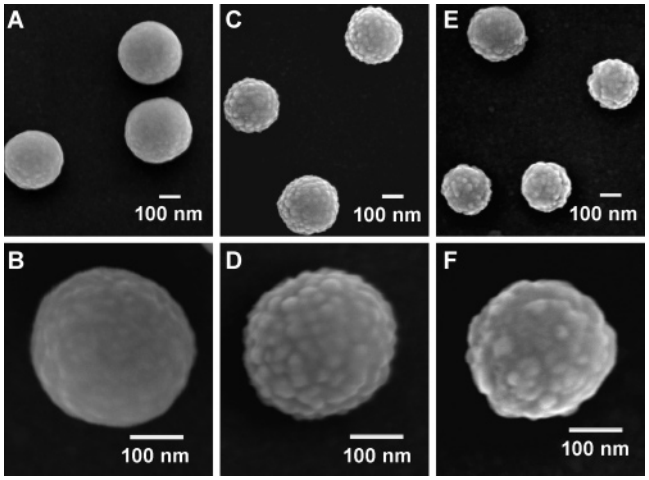

Figure 2. Surface morphological changes during etching: High-resolution SEM images of the Au nanoshells before etching(A, B) and after immersed in 50 mM cysteamine for (C, D) 1 h and (E, F) 2 h. The whole etching process can be divided into three stages: relatively smooth nanoshells, rough nanoshells, and isolated Au islands attached on the silica surface.

around 400 nm, which is partially due to the interband transition of Au clusters attached on the silica surface, and partially characteristic of the Rayleigh scattering of the silica nanoparticle core. The observed increase in surface roughness is most likely the result of preferential etching at particular crystalline facets of the polycrystalline Au shell layers. This is supported by analogous etching experiments performed on single crystalline solid Au nanoparticles. When solid Au nanoparticles were exposed to the cysteamine solution, the average diameter of the particles was seen to decrease; however, no roughening was observed on the surface of the nanoparticles (see Figure S1 in Supporting Information).

We studied this etching process as a function of solution pH, cysteamine concentration, and the presence of dissolved oxygen. It was determined that the rate of this etching process is pH dependent. Plots of the plasmon peak position as a function of exposure time (Figure S2 in Supporting Information) illustrate that the etching process proceeds most rapidly at high pH, more slowly at neutral pH, and no etching is observed at acidic pH. The overall rate of etching was determined to be a first-order process with respect to the concentration of cysteamine (see Figure S3 in Supporting Information). Dissolved oxygen in the aqueous cysteamine solution also plays a crucial role in the etching process. When the cysteamine solution was purged with N_2 gas to eliminate the dissolved oxygen, there was no detectable etching even after 4 h (see Figure S4 in Supporting Information). These factors provide important tools to regulate and control the extent of this chemical modification process and thereby controllably tailor the surface roughness and plasmonic properties of these nanostructures.

Three-dimensional finite difference time domain (FDTD) calculations were employed to more accurately relate the effects of this chemical restructuring on both the far-field and near-field optical properties of Au nanoshells. The FDTD method is a powerful approach that has recently been shown to be highly useful in the study of the electromagnetic properties of metallic nanostructures of almost arbitrary complexity.[35−39] In our simulations, the nanoshell surface texture was generated using a random number algorithm and the Drude dielectric function was used for the numerical results.[35] In Figure 3, the far-field spectra are shown for an Au nanoshell of inner and outer shell radii $(r_1, r_2) = (92, 128)$ nm at various stages in the chemical

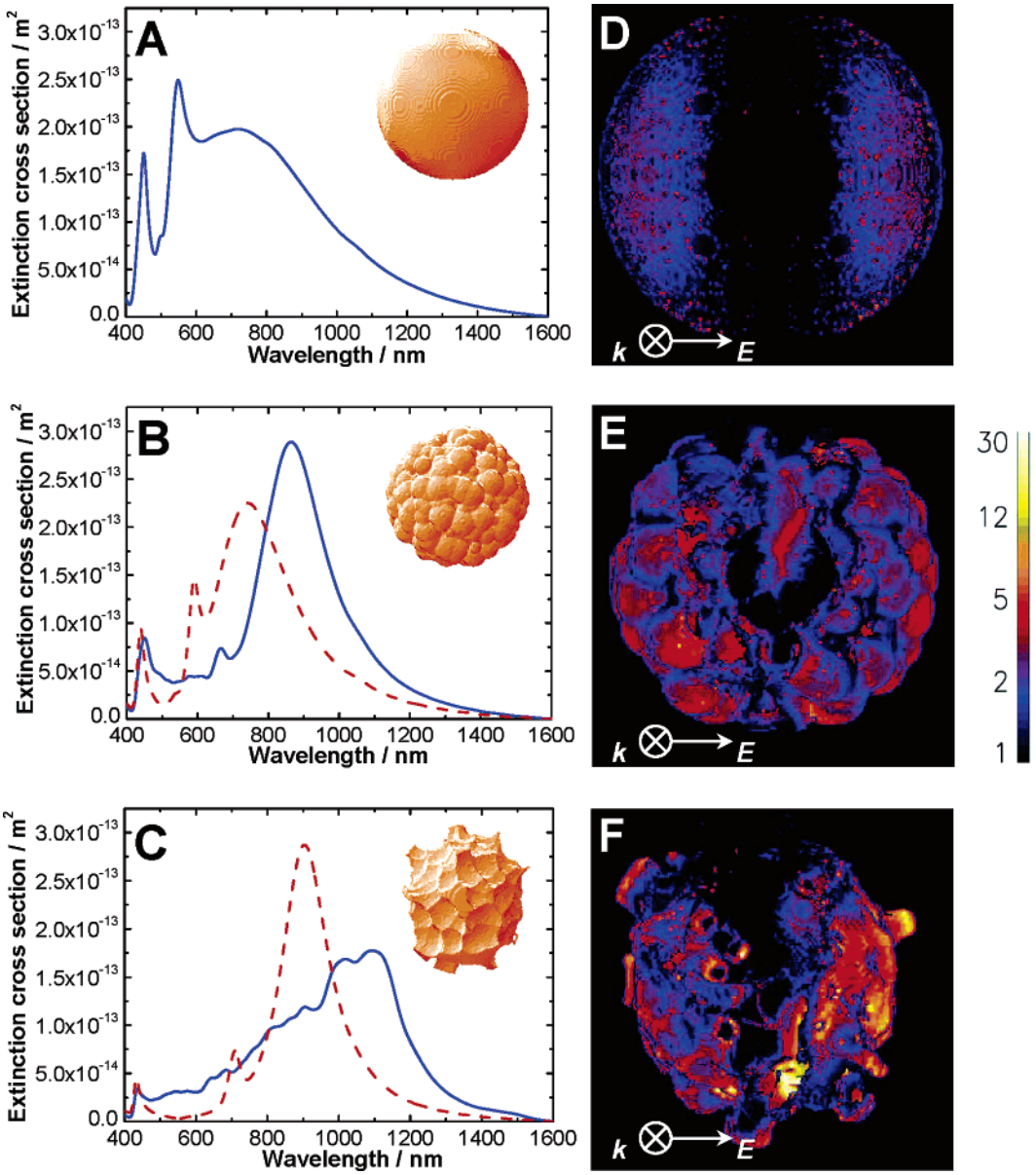

Figure 3. FDTD simulations of the far-field and near-field plasmoinc properties of a Au nanoshell at different stages during etching: Calculated far-field extinction cross section of (A) a (r_1, r_2) = (92, 128) smooth Au nanoshell. (B) Far-field extinction cross section of a rough but complete nanoshell (solid curve) and a smooth nanoshell (92, 110) with the same Au mass (dashed curve). The rough nanoshell was simulated by randomly adding 15−30 nm sized bumps on the surface of smooth nanoshell with 92 nm core radius and 6 nm shell thickness. (C) Far-field extinction cross section of isolated islands (solid curve) and a smooth nanoshell (92, 100) with the same Au mass (dashed curve). The isolated islands were simulated by randomly removing 82% gold from a smooth nanoshell with core radius of 92 nm, shell thickness of 36 nm and etching it all the way down to the core. The insets are the corresponding three-dimensional cartoon illustrations of the simulated objects. Near-field contours under the nanoshell resonance illuminations: (D) smooth nanoshell, λ = 718 nm; (E) rough nanoshells, λ = 861 nm; (F) isolated islands, λ = 1094 nm.

texturing process. Figure 3A−C show the theoretically calculated extinction spectra of a smooth nanoshell (A), a roughened but continuous nanoshell (B), and a nanoshell with a pitted and extensively etched Au surface (C). Parts B and C of Figure 3 also show the theoretical extinction spectrum for smooth shells with same Au mass as the corresponding roughened nanoshells. Due to the 92 nm core size, the smooth nanoshell shown in Figure 3A supports several multipole plasmon resonances,[40] a dipole resonance at ∼720 nm, a quadrupole resonance at ∼550 nm, and an octupole resonance at ∼460 nm. Due to the contributions of interband transitions in the Au layer at wavelengths shorter than 500 nm, the octupole plasmon would be highly damped and not discernible experimentally. The plasmon peaks red shift progressively as the smooth nanoshell is slowly roughened, as seen in Figure 3B. Even with significant texturing of the shell layer (Figure 3B), the nanostructure's plasmon response is largely preserved, although its higher order multipolar resonant modes have clearly been suppressed by the changes in its surface morphology. The nanostructure's far-field optical response has become more dipolar in character, and its plasmon resonant frequency is essentially preserved. The surface plasmon resonance peak of the rough nanoshell intensifies and red shifts compared to that of a smooth nanoshell with the same Au mass. For an extensively roughened shell with the presence of pits and cusps on the shell surface, the plasmon peak becomes significantly broadened and its intensity decreases as illustrated in Figure 3C. This is also in agreement with the experimental observation that there is no significant broadening of the plasmon spectrum of the nanoshells in etchant solution until after 90 min (Figure 1A). It indicates that conversion from rough yet continuous nanoshells into nanoshells with broken island shell layers probably takes place after etching for 90 min.

The calculated near-field contours of the smooth nanoshell, rough nanoshell and isolated islands under their resonance illuminations are shown in Figure 3D−F. Compared to the smooth nanoshell, both the textured nanoshell and the nanoshell with the disrupted shell layer possess local-field enhancements larger than are evident for a smooth nanoshell. Comparison of surface enhanced Raman scattering (SERS) intensities from adsorption of a *p*-mercaptoaniline monolayer on smooth vs textured nanoshells results in an observable increase in SERS signal of less than a factor of 10. It is likely that the SERS signal from the molecules affected by the highly localized "hot spots" on a textured nanoshell surface is not appreciably larger than the SERS signal from the total number of molecules on an untextured nanoshell surface.[41]

In conclusion, we report a chemical etching method for the controlled roughening of the surface topography of Au nanoshells. We have also examined, both experimentally and theoretically using FDTD simulations, how the plasmonic properties of Au nanoshells are modified by the induced modifications in nanoscale surface roughness. Roughened subwavelength nanostructures are of great fundamental interest, because they are extensively found in biological and environmental systems. Such a controlled method for introducing local roughness onto a nanoparticle surface may be useful in understanding how texturing on this length scale may affect the light scattering properties of other "rough" nanostructures that may occur in nature, such as subcellular organelles or atmospheric dust particles. Moreover, the precise role of the surface field on textured nanostructures relates directly to our ability to control and optimize chemical or biological sensing based on surface enhanced spectroscopies and, therefore, is attracting widespread interest for potential applications.

Experimental Section

Tetraethyl orthosilicate (TEOS, 99.9999%), (3-aminopropyl)-triethoxysilane (APTES), tetrachloroauric acid, and poly(4-vinylpyridine) (160 000 MW) were obtained from Sigma-Aldrich (St. Louis, MO). Ammonium hydroxide and ethanol were obtained from Fisher Scientific (Hampton, NH). Ultrapure water (18.2 MΩ resistivity) was obtained from a Milli-Q water purification system (Millipore, Billerica, MA). Glass microscope slides were obtained from Gold Seal Products (Portsmouth, NH). All the chemicals were used as received without further purification. Extinction spectra were obtained using a Cary 5000 UV/vis/NIR spectrophotometer in the wavelength range 400−1600 nm. Scanning electron microscopy (SEM) measurements were performed using a JEOL 6500 scanning electron microscope.

The fabrication of Au nanoshells has previously been described in detail.[23] In brief, colloidal silica nanospheres prepared by the Stöber method were used as the core material. The radius of the silica particles used in the present studies was determined to be 93 ± 14 nm by scanning electron microscopy (SEM) and dynamic light scattering (DLS) measurements. The surface of the silica was functionalized with (3-aminopropyl)-triethoxysilane, to generate an amine moiety-coated silica surface, and decorated with tetrakis(hydroxymethyl)phosphonium chloride stabilized Au nanoparticles (~2 nm in diameter). The attached Au colloids act as nucleation sites for the further reduction of $AuCl_4^-$ ions by formaldehyde, leading to the formation of continuous Au nanoshells. The as-prepared nanoshells were washed through multiple steps of centrifugation and redispersion in Milli-Q water (Millipore).

Nanoshell films were prepared by immobilization of the particles on glass substrates functionalized with poly(vinylpyridine).[28] Briefly, glass slides were cleaned in piranha solution (sulfuric acid:hydrogen peroxide, 7:3) and immersed in a 1 wt % solution of PVP in ethanol for 24 h. (***Caution****: Piranha solution reacts violently with organic matter and should be handled with extreme care!*) The slides were rinsed thoroughly with ethanol and dried with N_2 gas. The PVP-functionalized slides were immersed in an aqueous solution of nanoshells for 1 h. Upon removal from the nanoshell solution, the films were rinsed with ethanol and dried with N_2. This resulted in a submonolayer of isolated nanoshells immobilized on the PVP functionalized glass surface. Chemical etching of the Au nanoshells was performed by immersing the Au nanoshell films in aqueous solutions of cysteamine under ambient air at room temperature in darkness.

Acknowledgment. G.P.G. holds the Evans Attwell-Welch Postdoctoral Fellowship made possible by the Robert A. Welch Foundation. This work was supported by Air Force Office of Scientific Research Grant F49620-03-C-0068, National Science Foundation (NSF) Grant EEC-0304097, National Aeronautics and Space Administration (NASA) Grant 68371, Robert A. Welch Foundation Grants C-1220 and C-1222, Army Research Office (ARO) Grant DAAD19-99-1-0315, and Multidisciplinary University Research Initiative (MURI) Grant W911NF-04-01-0203.

Supporting Information Available: Etching of solid gold nanospheres, effects of solution pH and cysteamine concentration on the etching rate, and the effects of dissolved oxygen on the etching. This material is available free of charge via the Internet at http://pubs.acs.org.

References and Notes

(1) Ebbesen, T. W.; Lezec, H. J.; Ghaemi, H. F.; Thio, T.; Wolff, P. A. *Nature* **1998**, *391*, 667.
(2) Kneipp, K.; Wang, Y.; Kneipp, H.; Perelman, L. T.; Itzkan, I.; Dasari, R. R.; Feld, M. S. *Phys. Rev. Lett.* **1997**, *78*, 1667.
(3) Pendry, J. B. *Phys. Rev. Lett.* **2000**, *85*, 3966.
(4) Maier, S. A.; Brongersma, M. L.; Kik, P. G.; Meltzer, S.; Requicha, A. A. G.; Atwater, H. A. *Adv. Mater.* **2001**, *13*, 1501.
(5) Jana, N. R.; Gearheart, L.; Murphy, C. J. *Chem. Commun.* **2001**, 617.
(6) Nikoobakht, B.; El-Sayed, M. A. *Chem. Mater.* **2003**, *15*, 1957.
(7) Yu, Y. Y.; Chang, S. S.; Lee, C. L.; Wang, C. R. C. *J. Phys. Chem. B* **1997**, *101*, 6661.
(8) Chen, S. H.; Fan, Z. Y.; Carroll, D. L. *J. Phys. Chem. B* **2002**, *106*, 10777.
(9) Maillard, M.; Giorgio, S.; Pileni, M. P. *Adv. Mater.* **2002**, *14*, 1084.
(10) Hao, E. C.; Kelly, K. L.; Hupp, J. T.; Schatz, G. C. *J. Am. Chem. Soc.* **2002**, *124*, 15182.
(11) Pastoriza-Santos, I.; Liz-Marzan, L. M. *Nano Lett.* **2002**, *2*, 903.
(12) Chen, S. H.; Carroll, D. L. *Nano Lett.* **2002**, *2*, 1003.
(13) Sun, Y. G.; Xia, Y. N. *Science* **2002**, *298*, 2176.
(14) Charnay, C.; Lee, A.; Man, S. Q.; Moran, C. E.; Radloff, C.; Bradley, R. K.; Halas, N. J. *J. Phys. Chem. B* **2003**, *107*, 7327.
(15) Love, J. C.; Gates, B. D.; Wolfe, D. B.; Paul, K. E.; Whitesides, G. M. *Nano Lett.* **2002**, *2*, 891.
(16) Chen, S. H.; Wang, Z. L.; Ballato, J.; Foulger, S. H.; Carroll, D. L. *J. Am. Chem. Soc.* **2003**, *125*, 16186.
(17) Hao, E.; Bailey, R. C.; Schatz, G. C.; Hupp, J. T.; Li, S. *Nano Lett.* **2004**, *4*, 327.
(18) Jin, R. C.; Cao, Y. W.; Mirkin, C. A.; Kelly, K. L.; Schatz, G. C.; Zheng, J. G. *Science* **2001**, *294*, 1901.
(19) Link, S.; Burda, C.; Nikoobakht, B.; El-Sayed, M. A. *J. Phys. Chem. B* **2000**, *104*, 6152.
(20) Aguirre, C. M.; Kaspar, T. R.; Radloff, C.; Halas, N. J. *Nano Lett.* **2003**, *3*, 1707.
(21) Jin, R. C.; Egusa, S.; Scherer, N. F. *J. Am. Chem. Soc.* **2004**, *126*, 9900.
(22) Aguirre, C. M.; Moran, C. E.; Young, J. F.; Halas, N. J. *J. Phys. Chem. B* **2004**, *108*, 7040.
(23) Oldenburg, S. J.; Averitt, R. D.; Westcott, S. L.; Halas, N. J. *Chem. Phys. Lett.* **1998**, *288*, 243.

(24) Nehl, C.; Grady, N.; Goodrich, G. P.; Tam, F.; Halas, N. J.; Hafner, J. *Nano Lett.* **2004**, *4*, 2355.
(25) Prodan, E.; Radloff, C.; Halas, N. J.; Nordlander, P. *Science* **2003**, *302*, 419.
(26) Radloff, C.; Halas, N. J. *Nano Lett.* **2004**, *4*, 1323.
(27) Jackson, J. B.; Westcott, S. L.; Hirsch, L. R.; West, J. L.; Halas, N. J. *Appl. Phys. Lett.* **2003**, *82*, 257.
(28) Jackson, J. B.; Halas, N. J. *Proc. Natl. Acad. Sci. U.S.A.* **2004**, *101*, 17930.
(29) Oldenburg, S. J.; Westcott, S. L.; Averitt, R. D.; Halas, N. J. *J. Chem. Phys.* **1999**, *111*, 4729.
(30) Hirsch, L. R.; Jackson, J. B.; Lee, A.; Halas, N. J.; West, J. *Anal. Chem.* **2003**, *75*, 2377.
(31) Sershen, S. R.; Westcott, S. L.; Halas, N. J.; West, J. L. *J. Biomed. Mater. Res.* **2000**, *51*, 293.
(32) Loo, C.; Lin, A.; Hirsch, L.; Lee, M. H.; Barton, J.; Halas, N.; West, J.; Drezek, R. *Technol. Cancer Res. Treatment* **2004**, *3*, 33.
(33) Hirsch, L. R.; Stafford, R. J.; Bankson, J. A.; Sershen, S. R.; Rivera, B.; Price, R. E.; Hazle, J. D.; Halas, N. J.; West, J. L. *Proc. Natl. Acad. Sci. U.S.A.* **2003**, *100*, 13549.
(34) Oldenburg, S. J.; Jackson, J. B.; Westcott, S. L.; Halas, N. *Appl. Phys. Lett.* **1999**, *75*, 2897.
(35) Oubre, C.; Nordlander, P. *J. Phys. Chem. B* **2004**, *108*, 17740.
(36) Krug, J. T.; Sanchez, E. J.; Xie, X. S. *J. Chem. Phys.* **2002**, *116*, 10895.
(37) Maier, S. A.; Kik, P. G.; Atwater, H. A. *Appl. Phys. Lett.* **2002**, *81*, 1714.
(38) Maier, S. A.; Kik, P. G.; Atwater, H. A. *Phys. Rev. B* **2003**, *67*, Art. No. 205402.
(39) Futamata, M.; Maruyama, Y.; Ishikawa, M. *J. Phys. Chem. B* **2003**, *107*, 7607.
(40) Oldenburg, S. J.; Hale, G. D.; Jackson, J. B.; Halas, N. J. *Appl. Phys. Lett.* **1999**, *75*, 1063.
(41) Oubre, C.; Nordlander, P. *J. Phys. Chem. B* 10.1021/jp044382x.